

A closer examination of the Fabry-Perot Interferometer

Bram J. J. Slagmolen²,
Karl G. Baigent¹

Supervisors: Dr Malcolm Gray¹
Dr David McClelland¹
Prof. Hans Bachor¹
ir. Frans Bouts²
drs W. J. Coenders²

*Department of Physics and
Theoretical Physics
ANU*

4th July 1997



¹ Department of Physics and
Theoretical Physics,
Australian National University,
Physics Dept., Faculty of Science,
ACT 0200, Australia



² Department of Applied Physics,
TH Rijswijk, Lange Kleiweg 4,
2288 GK Rijswijk, The Netherlands

Acknowledgments

As part of my study in Applied Physics, field of study Photonics, at the TH Rijswijk in The Netherlands I have to do a traineeship in the trade and industry. The TH Rijswijk is an institute for students to graduate in technical professional education at sub-university level. Normally this is done in the second half of the third year. Usually a student goes to a Dutch company to do the traineeship. I decided to do it at the other side of the World and came to Australia.

In answer to my request I got a letter from David McClelland in which he acknowledged my acceptance to The Australian National University in Australia. I would like to thank him very much for this decision which he discussed with Hans Bachor, to whom I owe many thanks.

Next I want to thank Frans Bouts, my supervisor in The Netherlands, for supporting my stay in Australia (he never complained). It was good to know there was someone who understands and support things like this. And I can't forget Wim Coenders, a great teacher and someone who does what he knows.

And then in the lab. Karl Baigent, who's doing a Masters, and with whom I did this experiment. It was fun, we had some useful discussions and I learned a lot. Daniel Shaddock, who's doing his PhD, with whom I surfed the internet, he also gave me some useful tips, especially at the end of my stay at uni.

My supervisor at the ANU was Malcolm Gray, or Mal for short. I think he is great and funny. He gave me a shipload of books to study in the beginning but they were worth it. He also has shiploads of ideas for the future, and maybe I'll be back.

Then there are my friends. Ben and Michelle, who I met at the department, for all the fun and their place in the house later on. And Joseph for the coffee in the beginning and the beer later in the avro. Derek, my house mate and English corrector for this report. And heaps of others who showed me a great time in Australia.

And of course, I thank my mum and dad for the great job they did 23 years ago.

Thanks all.

Abstract

Three cavities where design and setup with different mirror reflectivities. Each cavity has its own properties which where dependent on the mirror reflectivities. All the cavities where locked with the Pound-Drever locking technique to keep the cavity on resonance with the laser beam.

While the cavity was locked, the reflected signal from the cavity was analysed by a network analyser. The transmitted signal through the cavity was analysed by the spectrum analyser. These analyses were done for the three different cavities. All the properties which can be determined with the transmitted signal where determined with the reflected signal also. Except the coupling onto the cavity can only be determined with the reflected signal.

Contents

Chapter 1. Introduction	7
Chapter 2. Gaussian Beams	9
Chapter 3. Interferometers	11
3.1 Fabry-Perot Interferometer	11
Chapter 4. Modulation	17
4.1 Amplitude modulation	17
4.1.1 Optical amplitude modulation	18
4.2 Phase modulation	21
4.2.1 Optical phase modulation	26
4.3 Light modulation	27
Chapter 5. Detection of the signals	29
Chapter 6. Equipment and experimental setup	31
6.1 The laser	31
6.2 Other equipment	31
6.3 The optical cavities	33
6.3.1 Cavity design	33
6.3.2 Cavity alignment	35
6.4 Frequency locking	36
Chapter 7. Experimental results	39
7.1 Cavity properties determination	39
7.2 Mirror reflectivity	40
7.2.1 Calculations from the finesse	40
7.2.2 Calculations from the phase response	41
7.3 The calculations	42
Chapter 8. Conclusion	43
Bibliography	45

A closer examination of the Fabry-Perot Interferometer

Chapter 1.

INTRODUCTION

This report describes most of the theory which is involved with a Fabry-Perot interferometer. A Fabry-Perot interferometer can be used to measure very small changes in, for example, distance. A Fabry-Perot interferometer can also be used to remove frequency noise from a laser to make the beam very clean.

A Fabry-Perot interferometer is setup as two mirrors facing each other. A laser beam is incident on one of the mirrors. The first mirror transmits some of the incident laser beam, which bounces between the two mirrors. If the light hits the first mirror again, in the optimum setup, it will interfere with the incident laser beam.

The primary aim of this experiment is to compare the information available in the transmitted and reflected signals. In some circumstances however there is no access to the transmitted beam (eg. with a super high finesse cavity, or when a cavity is used as a mode cleaner where beam splitting the transmitted beam is unacceptable due to the induced wavefront errors).

The people at the gravitational wave group at the Physics department are very experienced with this kind of experiments. All the equipment we needed was available.

The first six chapters describe the theory for the experiment. Most of the theory is clearly explained, and references to original papers are provided for more detailed information.

In chapter 7 the results from the experiment are presented, with the conclusion in chapter 8.

When working in the laboratory we kept a logbook wherein we note all results and changes. After a few months most of the results were analysed. Karl is starting to write a paper for publication based on this experimental data.

A closer examination of the Fabry-Perot Interferometer

Chapter 2.

GAUSSIAN BEAMS

To calculate the beam parameters through an optical system the free space Gaussian mode propagation is used [1][2]. It describes the position and width of the beam, the Gaussian beam intensity distribution is given by

$$I_{(r)} = I_0 e^{-\frac{2r^2}{w_0^2}} \quad (1)$$

where r is the radius of the beam waist at different positions and w_0 is the radius of the beam waist at the point of I_0/e^2 . In Fig. 1 the distribution is displayed graphically.

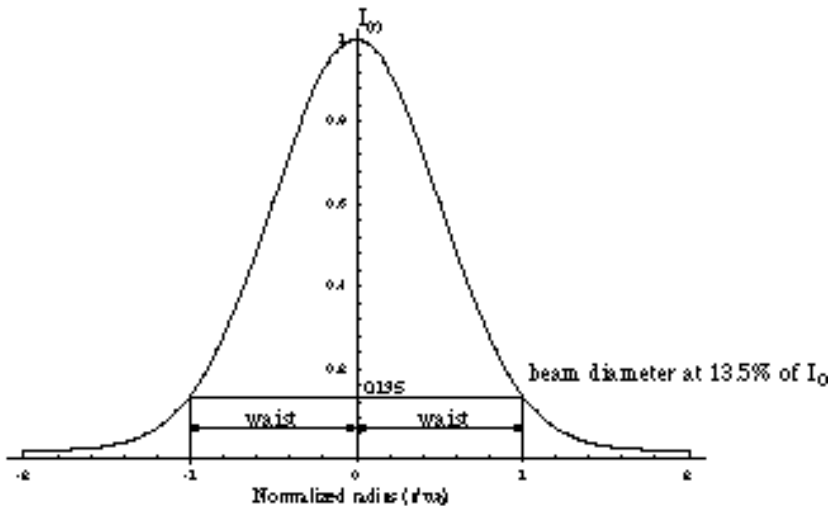


Figure 1. The Gaussian intensity distribution.

Because of the unique self-Fourier Transform characteristic of the Gaussian beam only the radius of the waist and the radius of curvature of the wavefront change through an optical system. These parameters can be calculated with

$$w_{(x)}^2 = w_0^2 \left[1 + \left(\frac{x}{w_0} \right)^2 \right] \quad (2)$$

$$R_{(x)} = x \left[1 + \left(\frac{w_0^2}{x^2} \right)^2 \right] \quad (3)$$

where λ is the wavelength, $R_{(x)}$ the radius of curvature of the wavefront and $w_{(x)}$ the beam radius.

A closer examination of the Fabry-Perot Interferometer

The beam size increases, slowly at first, then faster, eventually increasing proportionally to x . The wavefront radius of curvature, which is infinite at $x=0$, will become finite and initially decrease with x . There is one point in the beam where the Gaussian beam radius is at its smallest and where the Gaussian beam curvature is infinite, this point is called the ‘waist’. Indicated in Fig. 1, the Gaussian beam has a finite beam width which smoothly transits into a light cone of fixed numerical aperture. The parameter w_0 is called the Gaussian beam radius (waist), at which the intensity has decreased to $1/e^2$ or 0.135 of it’s original intensity.

The distance from $x=0$, where the wavefront of radius of curvature is infinite, to $x=z$, where the wavefront curvature is at its minimum, is called the ‘Rayleigh range’ and can be calculated by

$$z = z_R \equiv \frac{w_0^2}{\pi} \quad (4)$$

The Rayleigh range [3], z_R , is also the distance which the beam travels from the waist before the diameter increases by $\sqrt{2}$, and the beam area doubles. (see Fig. 2)

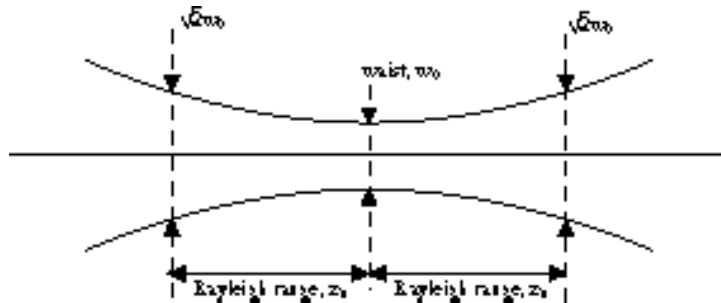


Figure 2. The Rayleigh range and the waist position of a Gaussian beam.

Chapter 3.

INTERFEROMETERS

The simplest kind of optical resonators consist of just two reflective surfaces [4]. The mirrors are curved, and generally the surfaces are coated. If the curvatures of these two mirrors corresponds to a stable periodic focusing system, then these mirrors can, in essence, trap a set of lowest-order and higher-order Gaussian modes or beams that will bounce back and forth between the two mirrors to form a stable, self repeating pattern.

Assume there is a Gaussian beam, with a certain waist size and waist location, in a cavity. If the radii of curvature of the mirrors is exactly matched to the wavefront radii of the Gaussian beam at those two points, and if the physical size of the mirrors is substantially larger than the Gaussian beam, each of these mirrors will reflect the Gaussian beam exactly back on itself, with exactly reversed wavefront curvature and direction. The two mirrors can thus trap the Gaussian beam as a standing wave.

3.1 Fabry-Perot Interferometer

The simplest form of an interferometer is the Fabry-Perot Interferometer (FPI), which consists of two partially transparent mirrors. The classical form is a resonator with two flat, parallel mirrors. Generally these mirrors are highly reflective, up to 99%, in order to reduce the optical bandwidth. Multilayer dielectric coatings deposited on quartz (or glass BK 7) substrates are commonly used as high-performance mirrors [5][6].

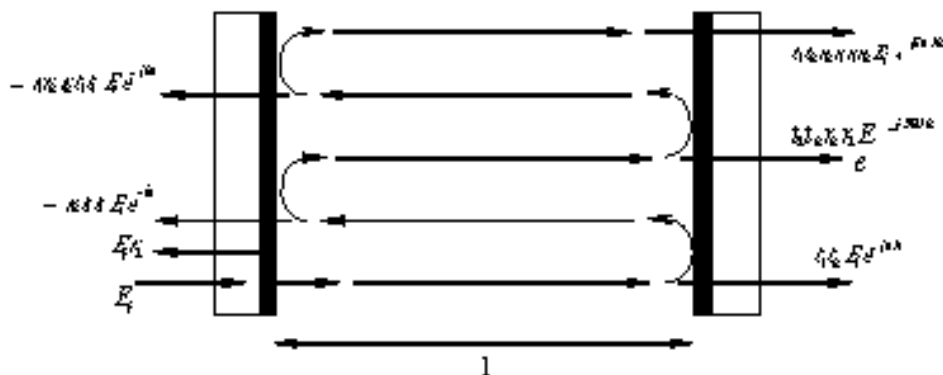


Figure 3. Fabry-Perot cavity.

In Fig. 3, the following definitions are made:

r_1 = amplitude reflection coefficient of the input mirror on the substrate side

$-r_1$ = amplitude reflection coefficient of the input mirror on the cavity side

- r_2 = amplitude reflection coefficient of the rear mirror on the cavity side
- t_1 = amplitude transmission coefficient of the input mirror
- t_2 = amplitude transmission coefficient of the rear mirror

There are many ways to calculate the characteristics of a FPI. The incident electric field E_i is partially reflected at mirror 1 with a factor r_1 and partially transmitted with a factor t_1 . When the transmitted field passes mirror 2, it appears delayed and multiplied with t_2 . The incident electric field E_i can be written as $E_i = E_0 \cdot e^{i(\Delta t - kz)}$, the ratio E_r/E_i is described by

$$\begin{aligned} \frac{E_r}{E_i} &= t_1 t_2 e^{\Delta i \Delta / 2} + t_1 t_2 r_2 r_1 e^{\Delta i 3 \Delta / 2} + t_1 t_2 r_2 r_1 r_2 e^{\Delta i 5 \Delta / 2} + \dots \\ &= t_1 t_2 e^{\Delta i \Delta / 2} \prod_{n=0}^{\infty} (r_1 r_2 e^{\Delta i \Delta})^n \\ &= \frac{t_1 t_2 e^{\Delta i \Delta / 2}}{1 - r_1 r_2 e^{\Delta i \Delta}} \equiv \bar{E}_T \end{aligned} \quad (5)$$

wherein $\Delta = 2\pi n l/c$ is the round trip phase shift of the light circulating in the cavity. Here the transmitted field E_T is written in complex notation. Similarly the reflected field E_R is given by:

$$\begin{aligned} \frac{E_r}{E_i} &= r_1 r_2 t_1 t_2 e^{\Delta i \Delta / 2} r_1 r_2 r_2 t_1 t_2 e^{\Delta i 2 \Delta / 2} r_1 r_2 r_1 r_2 r_2 t_1 t_2 e^{\Delta i 3 \Delta / 2} \dots \\ &= r_1 r_2 t_1 t_2 \prod_{n=0}^{\infty} (r_1 r_2)^n e^{\Delta i n \Delta} \\ &= \frac{r_1 r_2 (r_1^2 + t_1^2) e^{\Delta i \Delta / 2}}{1 - r_1 r_2 e^{\Delta i \Delta}} \equiv \bar{E}_R \end{aligned} \quad (6)$$

E_R is also written in complex notation.

The mirrors have absorption losses. The reflection coefficients r_i and r_2 are related to the mirror transmission t and absorption a by

$$r_i^2 + t_i^2 + a_i^2 = 1 \quad (7)$$

Eq. (6) can then be rewritten

$$\bar{E}_R = \frac{r_1 r_2 (r_1^2 + t_1^2) e^{\Delta i \Delta / 2}}{1 - r_1 r_2 e^{\Delta i \Delta / 2}} = \frac{r_1 r_2 (1 - a_1^2) e^{\Delta i \Delta / 2}}{1 - r_1 r_2 e^{\Delta i \Delta / 2}} \quad (8)$$

In this equation, if $r_2(1-a_1^2) > r_1$ then the numerator is negative and there is an overcoupled cavity. The phase of the reflected field shifts -360° when the cavity is going through resonance. If $r_2(1-a_1^2) < r_1$ there is an undercoupled cavity and the phase moves up and down less than $\pi/2$ radians. If $r_2(1-a_1^2) = r_1$ then the cavity is impedance matched. The phase moves from 0 to $-\pi/2$ and from $+\pi/2$ back to 0. A symmetric lossless cavity is impedance matched. Losses in the mirrors mean that symmetric cavities are undercoupled.

In Fig. 4 the transmitted and reflected fields are plotted. The absorption in the mirrors is constant, while the reflectivity coefficient of the front mirror is changed. The mirrors are set up as an overcoupled cavity. The graphs for an undercoupled cavity are shown in Fig. 5, where the reflectivity of the rear mirror varies.

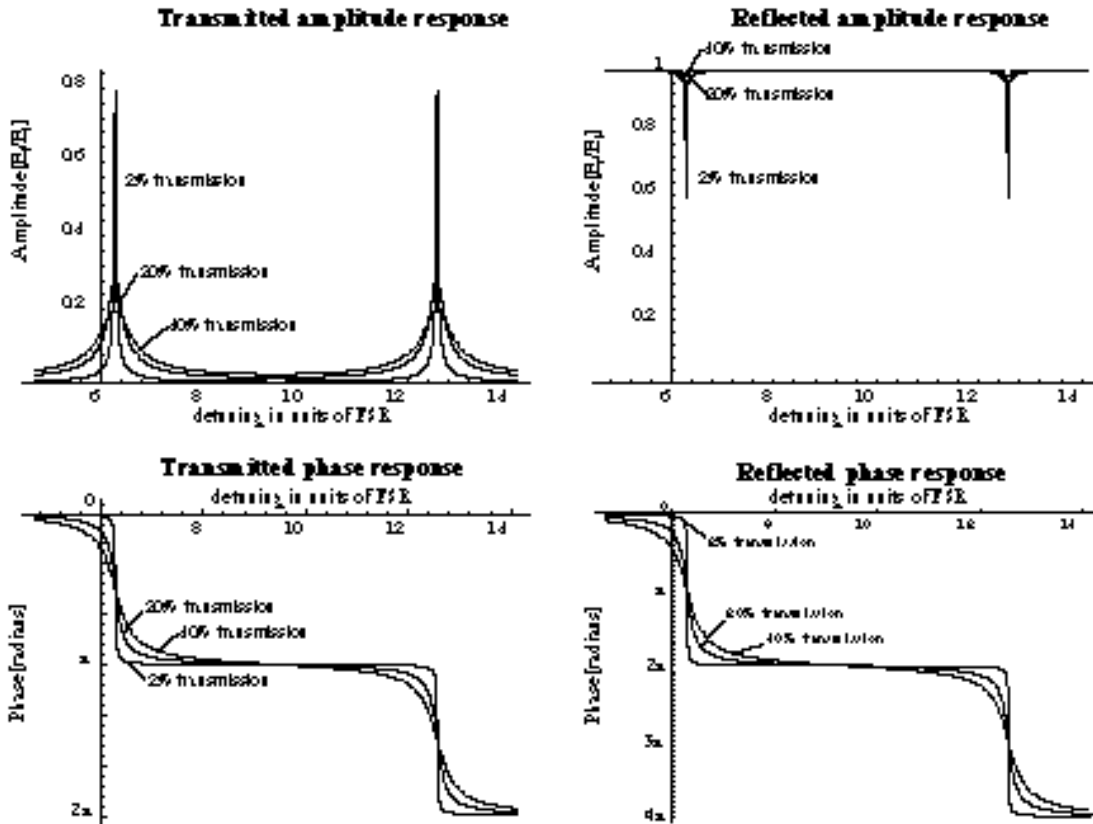


Figure 4. Overcoupled cavity, the absorption in the mirrors is $A_1 = A_2 = 10^{-4}$, and the transmission of the rear mirror is 0.5%. The transmission of the front mirror is shown in the figure.

The amplitude coefficient of transmission and reflection can be rewritten in complex exponential notation as

$$E_x = A_{\square} e^{i \square \square} \quad (9)$$

If A, B and C are defined as

$$A^2 = (1 \square A_1 \square T_1)$$

$$B^2 = (1 \square A_2 \square T_2)(1 \square A_1)^2$$

$$C^2 = (1 \square A_1 \square T_1)(1 \square A_2 \square T_2)$$

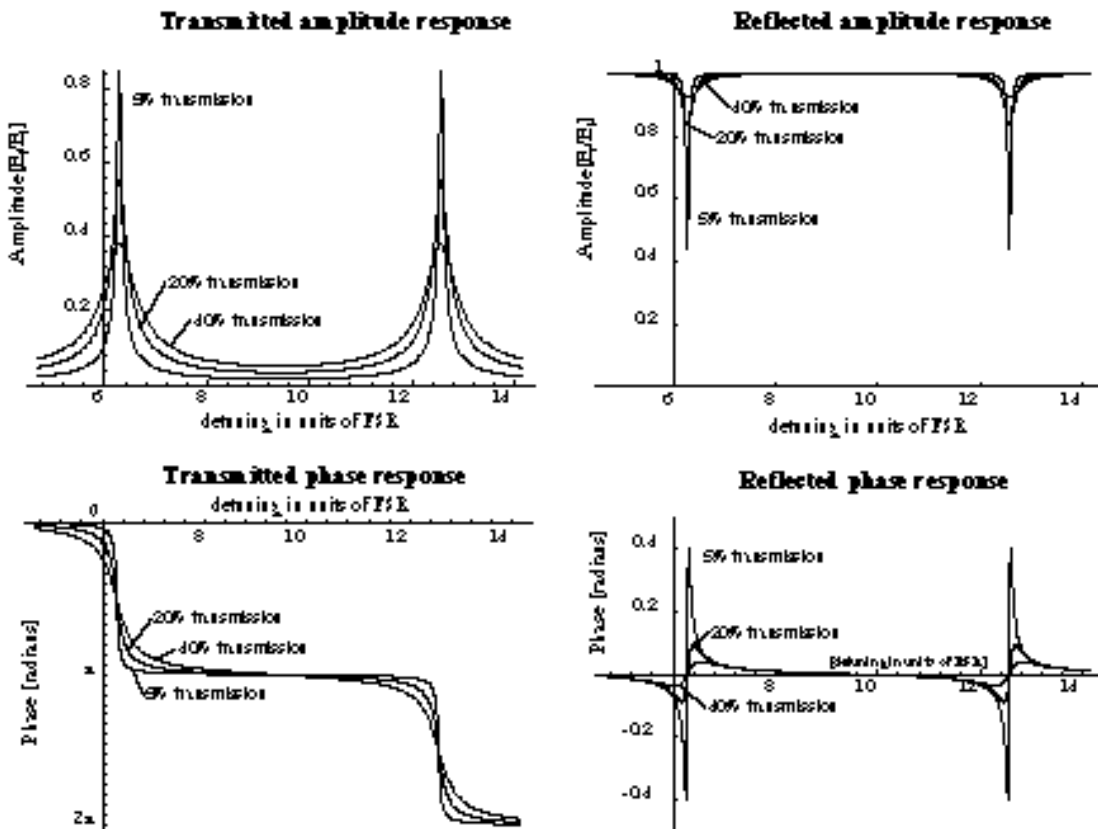


Figure 5. Undercoupled cavity, the absorption in the mirrors is $A_1 = A_2 = 10^{-4}$, and the transmission of the front mirror is 2%. The transmission of the rear mirror is shown in the figure.

the transmitted field becomes

$$\bar{E}_{T,(l)} = \frac{T_1 T_2}{1 - 2C \cos(l) + C^2} \exp \left[i \left(\frac{1}{2} l \right) \tan^{-1} \frac{C \sin(l)}{1 - C \cos(l)} \right] \quad (10)$$

Similarly for the reflected field

$$\bar{E}_{R,(l)} = \frac{A^2 - 2AB \cos(l) + B^2}{1 - 2C \cos(l) + C^2} \exp \left[i \tan^{-1} \frac{B \sin(l)}{A - B \cos(l)} \right] \tan^{-1} \frac{C \sin(l)}{1 - C \cos(l)} \quad (11)$$

In terms of the intensity the electric field of the transmission and reflection are as follows

$$R_i = |r_i|^2 \quad T_i = |t_i|^2 \quad (12)$$

$$I_T = \frac{T_1 T_2}{1 + R_1 R_2 - 2\sqrt{R_1 R_2} \cos(l)} \quad (13)$$

$$I_R = \frac{R_1 + (R_1 + T_1)^2 R_2 - 2\sqrt{R_1 R_2} (R_1 + T_1) \cos(l)}{1 + R_1 R_2 - 2\sqrt{R_1 R_2} \cos(l)} \quad (14)$$

Other parameters of a cavity are: the free-spectral-range (FSR), the frequency spacing between the adjacent longitudinal modes; the full-width-half-maximum (FWHM) of the transmitted field or the cavity bandwidth; and the finesse (F).

$$\text{FSR} = \frac{c}{2L} \quad (15)$$

$$FWHM = \frac{\text{FSR}}{F} \quad (16)$$

$$F = \frac{1/(R_1 R_2)^{1/4}}{1 - \sqrt{R_1 R_2}} \text{ (finesse)} \quad (17)$$

Chapter 3. Interferometers

Chapter 4.

MODULATION

Generally, modulation is the process by which a property or a parameter of a signal is varied in proportion to a second signal. The precise dependence is determined by the type of modulation employed. In amplitude modulation, the amplitude of a sinusoidal signal, whose frequency and phase are fixed, is varied in proportion to a given signal. This alters the given signal by translating its frequency components to higher frequencies.

4.1 Amplitude modulation^[7]

The equation of a general sinusoidal signal can be written as

$$\square(t) = a(t) \cos \square(t) \quad (18)$$

where $a(t)$ is the time-varying amplitude and $\square(t)$ is the time-varying angle. It is convenient to write $\square(t) = \square_c t + \square(t)$ so that

$$\square(t) = a(t) \cos[\square_c t + \square(t)] \quad (19)$$

Assume that $a(t)$ and $\square(t)$ are slowly varying compared to $(\square_c t)$. The term $a(t)$ is called the envelope of the signal $\square(t)$ and the term \square_c is called the carrier frequency; $\square(t)$ is the phase modulation of $\square(t)$.

In amplitude modulation, the phase term $\square(t)$ in Eq. (19) is zero (or a constant) and the envelope $a(t)$ is made proportional to the given signal $f(t)$. Letting the constant of proportionality be unity here, the follow equation will occur

$$\square(t) = f(t) \cos \square_c t \quad (20)$$

Applying the modulation property of the Fourier transform to Eq. (20), the spectral density of $\square(t)$ is

$$\square(\square) = \frac{1}{2} F(\square + \square_c) + \frac{1}{2} F(\square - \square_c) \quad (21)$$

The term $\cos \square_c t$ in Eq. (20) is called the carrier signal and $f(t)$ is called the modulating signal. The resultant signal, $\square(t)$, is called the modulated signal with $F(\square)$ as the Fourier transform of $f(t)$.

In the experiment a double-sideband large-carrier (DSB-LC) is used to modulate the signal. The signal can be described mathematically simply by adding a carrier term, $A \cos \Omega_c t$, to the modulated signal:

$$\square_{AM}(t) = f(t) \cos \Omega_c t + A \cos \Omega_c t \quad (22)$$

Applying the modulation property of the Fourier transform to Eq. (22), the spectral density of $\square_{AM}(t)$ is:

$$\begin{aligned} \square_{AM}(\Omega) = & \frac{1}{2} F(\Omega + \Omega_c) + \frac{1}{2} F(\Omega - \Omega_c) \\ & + A \delta(\Omega + \Omega_c) + A \delta(\Omega - \Omega_c) \end{aligned} \quad (23)$$

The spectral density of $\square_{AM}(t)$ is the same as the modulated signal $f(t) \cos \Omega_c t$ with the addition of impulses at $\pm \Omega_c$. This is illustrated in Fig.6.

4.1.1 Optical amplitude modulation

The experiment was setup as illustrated in Fig. 7. The beam which goes in to the Pockels cell is vertically polarised, this is done by a polarizer where necessary. The incoming beam can be described by:

$$E = \hat{y} e^{i \Omega_c t} \quad (24)$$

The incident beam which goes in to the Pockels cell will be split in to two directions, the two axes of the Pockels cell [9].

$$E_{inc} = \frac{\hat{k}}{\sqrt{2}} + \frac{\hat{l}}{\sqrt{2}} \quad (25)$$

where \hat{k} and \hat{l} describe the axes of the Pockels cell. After the Pockels cell, at $z=l$, there is a phase difference between the two components, and this is called the retardation (\square). This is caused by voltage across the Pockels cell.

$$E_l = \frac{\hat{k}}{\sqrt{2}} e^{i \square} + \frac{\hat{l}}{\sqrt{2}} e^{\square i \square} \quad (26)$$

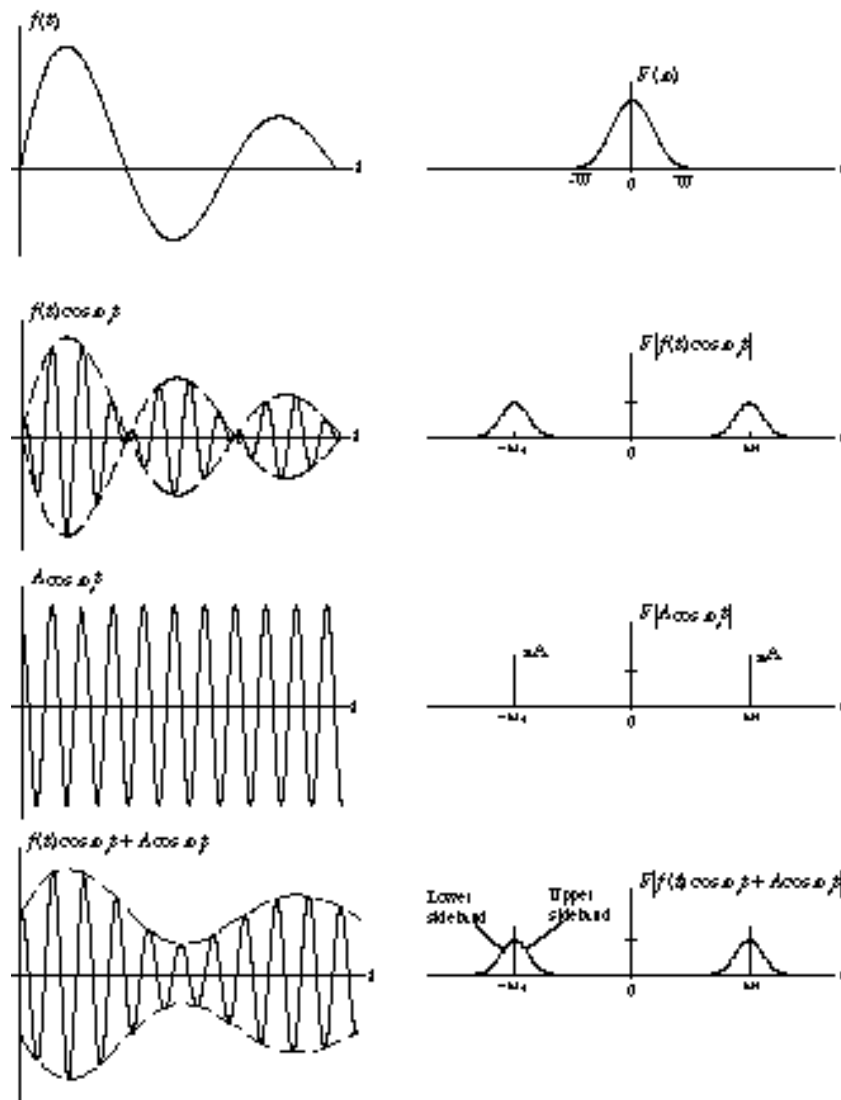


Figure 6. Amplitude modulation of a signal $f(t)$ and the spectral density of the modulation.

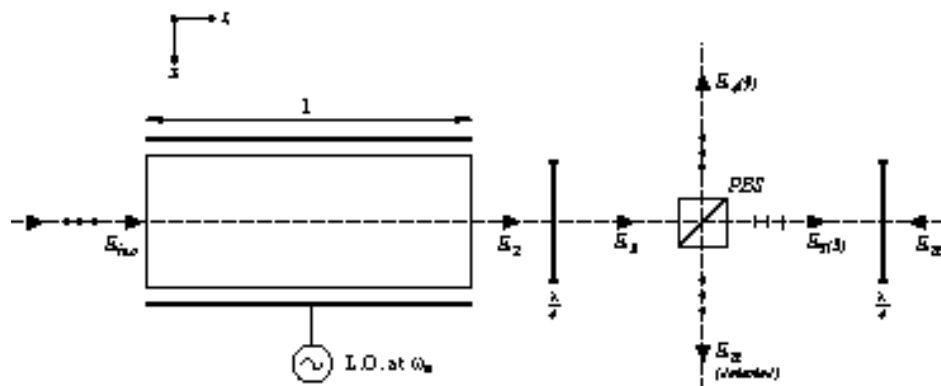


Figure 7. The optical amplitude modulation setup. The Pockels cell is the main component for the modulation and the quarter-waveplates are present to make circular polarised light into linear polarised light for the polarised-beamsplitter. The Pockels cell is driven by the modulation frequency ω_m . The reflected light (E_R) from the front mirror of the cavity is used to determine the kind of cavity and to lock the cavity.

The quarter-waveplate increases the retardation by 45 degrees. The electric field after the waveplate is described by:

$$E_2 = \frac{\hat{k}}{\sqrt{2}} e^{i\frac{\pi}{4}} e^{i\Box} + \frac{\hat{l}}{\sqrt{2}} e^{\Box i\frac{\pi}{4}} e^{\Box i\Box} \quad (27)$$

The polarised-beamsplitter will split the beam into its horizontal and vertical components. The vertical component (\hat{y}) is reflected by the beamsplitter, the horizontal component (\hat{x}) is transmitted. After the beamsplitter the equation of E_3 (the horizontal component) is described by:

$$E_3(\hat{x}) = \frac{e^{i\frac{\pi}{4}+i\Box}}{2} - \frac{e^{\Box i\frac{\pi}{4} i\Box}}{2} \quad (28)$$

Similarly for E_4 , the vertical component:

$$E_4(\hat{y}) = \frac{e^{i\frac{\pi}{4}+i\Box}}{2} + \frac{e^{\Box i\frac{\pi}{4} i\Box}}{2} \quad (29)$$

Eq. (28) rewritten with $\frac{i}{2} [e^{i\Box} - e^{\Box i\Box}] = \sin \Box$:

$$\begin{aligned} E_3(\hat{x}) &= i \sin \frac{\Box}{4} + \frac{\Box}{4} \\ &= e^{i\frac{\pi}{2}} [\sin(\frac{\Box}{4}) \cos(\Box) + \cos(\frac{\Box}{4}) \sin(\Box)] \\ &= \frac{e^{i\frac{\pi}{2}}}{\sqrt{2}} [\cos(\Box) + \sin(\Box)] \end{aligned} \quad (30)$$

for small retardation's (\Box):

$$E_3(\hat{x}) = \frac{e^{i\frac{\pi}{2}}}{\sqrt{2}} (1 + \frac{\Box^2}{2} + \Box) \frac{e^{i\frac{\pi}{2}}}{\sqrt{2}} (1 + \Box) e^{i\Box_c t} \quad (31)$$

The incident beam on the cavity is amplitude modulated as E_3 . The reflected signal can be written as:

$$\begin{aligned} E_{inc,\sin} &= E_3(\hat{x}) = \frac{e^{i\frac{\pi}{2}}}{\sqrt{2}} e^{i\Box_c t} (1 + \Box) \\ &= \frac{e^{i\frac{\pi}{2}}}{\sqrt{2}} e^{i\Box_c t} (1 + \Box_m \sin \Box_m t) \\ &= \frac{e^{i\frac{\pi}{2}}}{\sqrt{2}} \left[e^{i\Box_c t} + \frac{\Box_m e^{i\Box_c t}}{2i} \left[e^{i\Box_m t} - e^{-i\Box_m t} \right] \right] \\ &= \frac{e^{i\frac{\pi}{2}}}{\sqrt{2}} \left(e^{i\Box_c t} + \frac{\Box_m}{2i} e^{i(\Box_c + \Box_m)t} - \frac{\Box_m}{2i} e^{i(\Box_c - \Box_m)t} \right) \end{aligned} \quad (32)$$

where in $\Box_m = \Box(V_m/V_\Box)$, and V_\Box is the voltage yielding a retardation of $\Box = \Box$. And V_m is the maximum modulation voltage. This signal is driven by a sinusoidal.

For a cosinusoidal driven signal the equation is as follows (continuing from Eq. (30)):

$$\begin{aligned}
E_{inc,\cos} &= E_3(\hat{x}) = \frac{e^{i\frac{\pi}{2}}}{\sqrt{2}} e^{i\omega_c t} (1 + \square) \\
&= \frac{e^{i\frac{\pi}{2}}}{\sqrt{2}} e^{i\omega_c t} (1 + \square_m \cos \square_m t) \\
&= \frac{e^{i\frac{\pi}{2}}}{\sqrt{2}} \left[e^{i\omega_c t} + \frac{\square_m e^{i\omega_c t}}{2} \left[e^{i\omega_m t} + e^{-i\omega_m t} \right] \right] \\
&= \frac{e^{i\frac{\pi}{2}}}{\sqrt{2}} \left(e^{i\omega_c t} + \frac{1}{2} \square_m e^{i(\omega_c + \omega_m)t} + \frac{1}{2i} \square_m e^{i(\omega_c - \omega_m)t} \right)
\end{aligned} \tag{33}$$

In Fig. 8 the spectral densities are displayed from the sinusoidal and cosinusoidal signals. These signals are both in the incident signal.

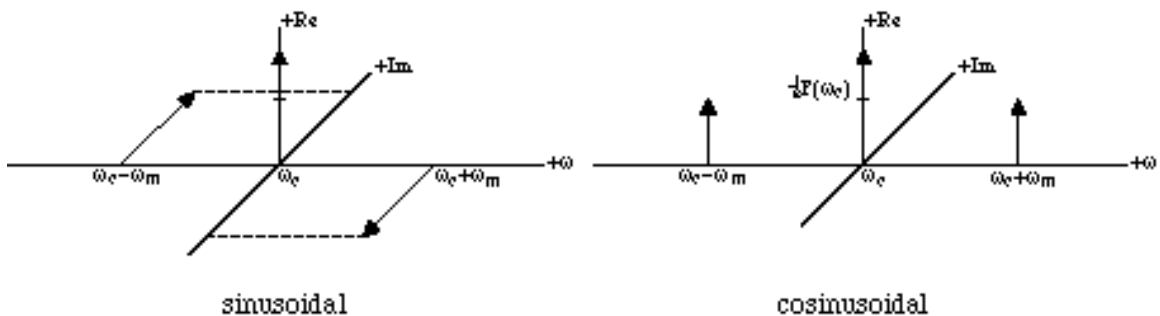


Figure 8. The Fourier transform spectral density of the two modulated signals. The sidebands of the spectral density are important as these are detected.

4.2 Phase modulation^[8]

In the previous chapter the amplitude of a signal is varied to get a modulated signal. Recalling Eq. (19)

$$\square(t) = a(t) \cos[\omega_c t + \square(t)]$$

$\square(t)$ is constant and $a(t)$ varied proportionally to $f(t)$. This introduces the concept of amplitude modulation. If $a(t) = A$ (a constant) and the phase $\square(t)$ is varied in proportion to $f(t)$, then the result is angle modulation.

The angle of a sinusoidal signal is described in terms of a frequency and/or a phase angle. If a sinusoid has a constant angular rate ω_0 , then the frequency of the sinusoid is ω_0 radians per second. The phasor in Fig. 9 represents a constant amplitude sinusoid. This phasor has a magnitude A and a phase angle $\square(t)$. If $\square(t)$ increases linearly with time ($\square(t) = \omega_0 t$) the phasor has an angular rate, or frequency of ω_0 radians per second. If the angular rate is not constant, the relation between the instantaneous angular rate $\omega_i(t)$ and $\square(t)$ is described by

$$\square(t) = \int_0^t \omega_i(\square)d\square + \square_0 \tag{34}$$

Taking the derivative of both sides of Eq. (34)

$$\square_i(t) = \frac{d\square}{dt} \quad (35)$$

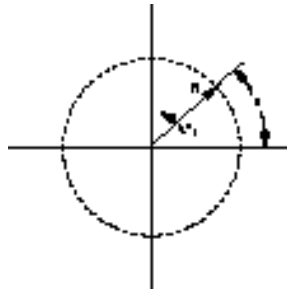


Figure 9. A general phasor representation.

If the phase angle $\square(t)$ is varied linearly with the input signal $f(t)$ then

$$\square(t) = \square_c t + k_p f(t) + \square_0 \quad (36)$$

where \square_c , k_p , \square_0 are constants. Where the phase is linearly related to $f(t)$, this type of angle modulation is called *phase modulation* (PM). The instantaneous frequency of this phase-modulated signal is described by

$$\square_i = \frac{d\square}{dt} = \square_c + k_p \frac{df}{dt} \quad (37)$$

Another possibility is to make the instantaneous *frequency* proportional to the input signal,

$$\square_i = \square_c + k_f f(t) \quad (38)$$

where \square_c , k_f are constants. Where the frequency is linearly related to $f(t)$, this type of angle modulation is called *frequency modulation* (FM). The phase angle of this frequency-modulation signal is described by

$$\square(t) = \int_0^t \square_i(\square) d\square = \square_c t + \int_0^t k_f f(\square) d\square + \square_0 \quad (39)$$

A comparison of Eqs. (36)-(39) shows that the PM and FM are closely related. In PM the phase angle of the carrier signal is varied linearly with the modulating signal. In FM the phase angle of the carrier signal is varied linearly with the integral of the modulating signal (see Fig. 10). Therefore, if the modulated signal $f(t)$ is integrated first and then used to phase modulate a carrier, a frequency-modulated signal will result.

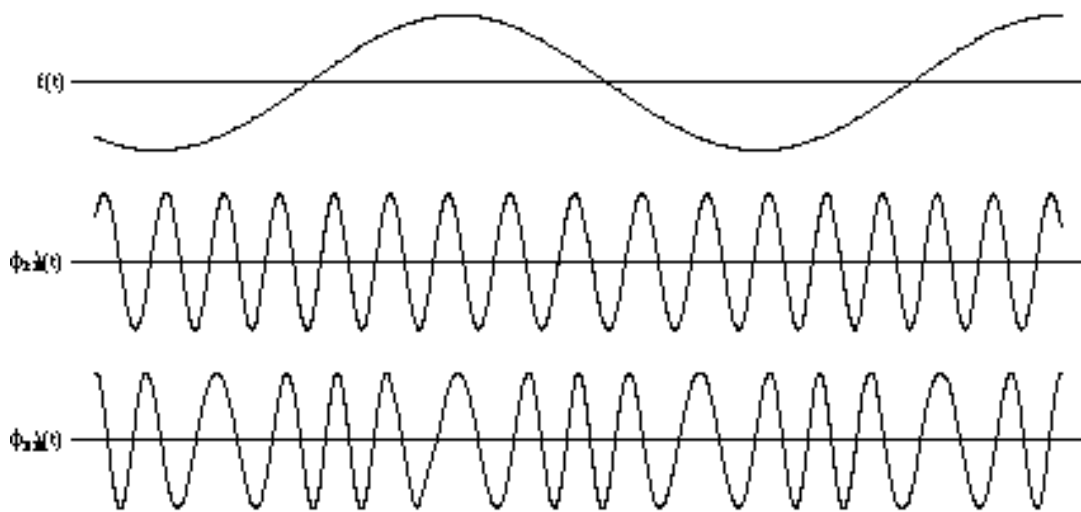


Figure 10. Examples of frequency and phase modulation.

Because frequency and phase modulation are so closely related, any variation in phase will necessarily result in a variation in frequency and vice versa. The essential difference between FM and PM is the nature of the dependency on the modulating signal. Therefore it is not possible to analytically evaluate the Fourier transform of a general FM waveform and so pure sinusoidal is explained here.

Continuing from a given signal (Eq. (20)),

$$f(t) = a \cos \Omega_m t \quad (40)$$

for FM,

$$\begin{aligned} \Omega_i(t) &= \Omega_c + ak_f \cos \Omega_m t \\ &= \Omega_c + \Omega \cos \Omega_m t \end{aligned} \quad (41)$$

where k_f is the frequency modulator constant, and $\Omega = ak_f$ and is called the *peak frequency deviation*. The phase of this FM signal is described by

$$\begin{aligned} \Omega(t) &= \int_0^t \Omega_i(\tau) d\tau \\ &= \Omega_c t + \frac{\Omega}{\Omega_m} \sin \Omega_m t \\ &= \Omega_c t + \Omega \sin \Omega_m t \end{aligned} \quad (42)$$

where $\Omega = \Omega / \Omega_m$, the *modulation index*. Ω is a dimensionless ratio of the peak frequency deviation to the modulating frequency, and serves as a guide to the behaviour of the carrier and sidebands. Using complex notation Eq. (42) can be rewritten as

$$\begin{aligned}\square_{FM}(t) &= \operatorname{Re}[Ae^{i\square t}] \\ &= \operatorname{Re}[Ae^{i\square_c t} e^{i\square \sin \square_m t}]\end{aligned}\quad (43)$$

The second exponential in Eq. (43) is a periodic function in time with a fundamental frequency of \square_m rad/sec. It can be expanded in a Fourier series

$$e^{i\square \sin \square_m t} = \sum_{n=0}^{+\infty} F_n e^{in\square_m t} \quad (44)$$

where

$$F_n = \frac{1}{T} \int_{-\frac{T}{2}}^{\frac{T}{2}} e^{i\square \sin \square_m t} e^{in\square_m t} dt \quad (45)$$

It is a function of n and \square , denoted by $J_n(\square)$, and is called the Bessel function of the first kind, of order n and argument \square . Now Eq. (44) can be rewritten as

$$e^{i\square \sin \square_m t} = \sum_{n=0}^{+\infty} J_n(\square) e^{in\square_m t} \quad (46)$$

and Eq. (43) becomes

$$\begin{aligned}\square_{FM}(t) &= \operatorname{Re} \left[A e^{i\square_c t} \sum_{n=0}^{+\infty} J_n(\square) e^{in\square_m t} \right] \\ &= A \sum_{n=0}^{+\infty} J_n(\square) \cos((\square_c + n\square_m)t)\end{aligned}\quad (47)$$

This can be expanded with the Bessel function to

$$\begin{aligned}\square_{FM}(t) &= A \{ J_0(\square) \cos \square_c t \\ &\quad + J_1(\square) [\cos(\square_c + \square_m)t - \cos(\square_c - 2\square_m)t] \\ &\quad + J_2(\square) [\cos(\square_c + 2\square_m)t + \cos(\square_c - 2\square_m)t] \\ &\quad + J_3(\square) [\cos(\square_c + 3\square_m)t - \cos(\square_c - 3\square_m)t] \\ &\quad + \dots \}\end{aligned}\quad (48)$$

From these results, it is evident that an FM waveform with sinusoidal modulation, in contrast to AM, has an infinite number of sidebands. However, the magnitude of the spectral components of the higher-order sidebands become negligible and, for all practical purposes, the power is contained within a finite bandwidth. The number of sidebands depends on the intended application and the fidelity requirements. A rule of thumb is that a

sideband is significant if its magnitude is equal to or exceeds 1% of the unmodulated carrier, i.e., if $J_n(\beta) \geq 0.01$.

There is no basic difference between the mechanisms involved in the generation of phase modulation (PM) and frequency modulation (FM). In fact, the only difference is that the phase in the modulated wavefront is proportional to the input signal amplitude in PM and to the integral of the input signal in FM.

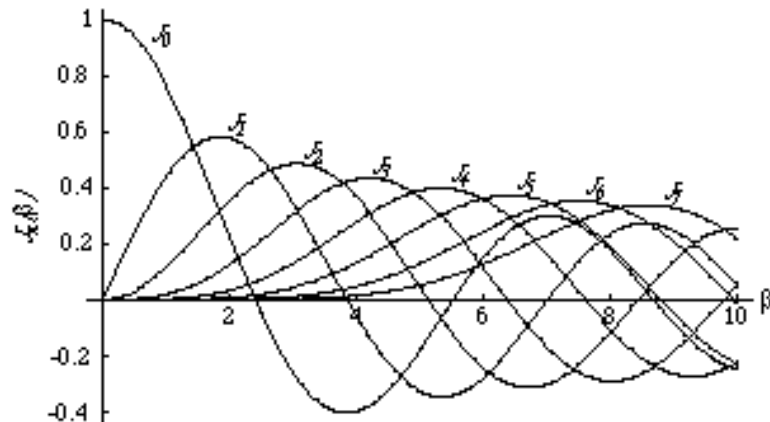


Figure 11. Plots of the Bessel function of the first kind. Notice that for small β and for higher n , the Bessel function $J_n(\beta)$ is negliblerer.

Continuing from Eq. (41) for PM the phase is described by

$$\begin{aligned} \phi(t) &= \omega_c t + ak_p \cos \omega_m t + \phi_0 \\ &= \omega_c t + \Delta \phi \cos \omega_m t + \phi_0 \end{aligned} \quad (49)$$

where $\Delta \phi$ is the peak phase deviation (in radians) and k_p the phase-modulator constant. The instantaneous frequency is described by

$$\begin{aligned} \dot{\phi}_i(t) &= \frac{d\phi}{dt} \\ &= \omega_c + ak_p \omega_m \sin \omega_m t \\ &= \omega_c + \Delta \phi \sin \omega_m t \end{aligned} \quad (50)$$

The peak frequency deviation in PM is proportional not only to the amplitude of the modulating wavefront but also to its frequency:

$$\Delta \phi = \begin{cases} ak_f & \text{for FM} \\ ak_p \omega_m = (\Delta \phi) \omega_m & \text{for PM} \end{cases} \quad (51)$$

This makes PM less desirable to transmit when $\Delta \phi$ is fixed. The role of the modulation index β remains the same as in FM. Formally, $\Delta \phi = ak_f = ak_p \omega_m = (\Delta \phi) \omega_m$, and proceed as if

the modulation were FM as far as bandwidth, sidebands, etc. are concerned. Note that the numerical value of Δ is the peak phase deviation, $\Delta\phi$, in the PM case.

4.2.1 Optical phase modulation^[5]

The phase modulation of the laser light is done by changing the optical path of the generated light through the laser crystal. The source of the laser light is a crystal in the diode pumped solid state ring laser. To modulate the light a piezo element is mounted to the crystal and this changes the physical size of the crystal. The modulation frequency is limited by the physical properties of the crystal (in the experiment $\sim 9.1\text{MHz}$).

The electric field of the incident light on the crystal can be described by

$$E_{inc} = Ae^{i\Delta_0 t} \quad (52)$$

where A is the amplitude of the electric field and Δ_0 is the laser frequency. As the physical size of the laser crystal change due to the piezo element by a voltage E_p the instantional frequency of the laser light leaving the crystal varies by $\Delta\Delta = E_p$. When E_p is driven by a sinusoidal signal

$$E_p = E_m \sin \Delta_m t \quad (53)$$

the electric field which leave the crystal can be described by

$$E_0 = Ae^{i(\Delta_0 t + \frac{\Delta_0}{c} \Delta \Delta \sin \Delta_m t)} \quad (54)$$

where Δ is the modulation index and depends on E_m , l , Δ_0 and the physical properties of the crystal. Using Eq. (48) the output electric field may be expand into

$$\begin{aligned} E_0 = & A\{J_0(\Delta)e^{i\Delta_0 t} \\ & + J_1(\Delta)[e^{i(\Delta_0 + \Delta_m)t} - e^{i(\Delta_0 - \Delta_m)t}] \\ & + J_2(\Delta)[e^{i(\Delta_0 + 2\Delta_m)t} + e^{i(\Delta_0 - 2\Delta_m)t}] \\ & + J_3(\Delta)[e^{i(\Delta_0 + 3\Delta_m)t} - e^{i(\Delta_0 - 3\Delta_m)t}] \\ & + \dots \} \end{aligned} \quad (55)$$

For small modulation depth the Bessel function decrease rapidly with increase order. Hence only the first order components are usually considered, this is displayed in Fig. 12.

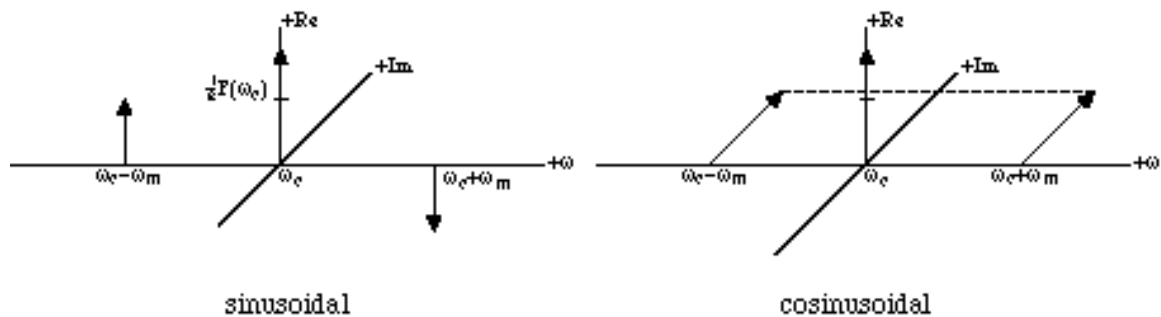


Figure 12. The Fourier transform spectral density of the phase modulated signal.

4.3 Light modulation

To measure the different parameters of the cavity the laser light has to be modulated. Direct light modulation of the laser's drive current causes dynamical effects on the emitted spectrum, such as changes in the peak wavelength, spectral bandwidth and the amplitude of the individual cavity modes. The smaller the number of the emitted modes, the larger these effects. The laser used in this experiment, a diode pumped solid state ring laser, can be frequency modulated but amplitude modulation has to be done with external components.

Chapter 5.

DETECTION OF THE SIGNALS

The intensity on the photodiode is proportional to the amplitude of the electric field squared (Eq. (31)). A photodiode is not able to detect any electric field phase changes. The photocurrent can be written as follow

$$\begin{aligned}
 I_p &= |E|^2 \\
 &= |E_0 + E_1 e^{i\Box_m t} + E_{\Box} e^{\Box i\Box_m t}|^2 \\
 &= |E_0|^2 + |E_1|^2 + |E_{\Box}|^2 \\
 &\quad + 2\text{Re}[E_1 E_1^* e^{i2\Box_m t}] \\
 &\quad + 2\text{Re}[(E_0 E_{\Box}^* + E_1 E_0^*) e^{i\Box_m t}]
 \end{aligned} \tag{56}$$

where $E_0 = iJ_0$ and $E_1 = E_{-1} = iJ_1$ are the Bessel functions of integer order. As illustrated in Fig. 11 higher Bessel functions than $n = 1$ are not significant for low \Box numbers. This is why only the first two Bessel functions, $J_0(\Box)$ and $J_1(\Box)$, are used.

The first three terms of Eq. (56) are responsible for the DC level of the signal, while the fourth term is at the beat frequency ($2\Box_m$). The last term describes the part of the signal used for analysis.

As shown in Fig 13, the RF photocurrent (I_p) is mixed with a local oscillator (L.O.) by a mixer (M). A mixer multiplied the two signals in the time domain. There are two signals coming from the LO (driven at \Box_m), one of them get a phase shift of 90° . There are two outputs from the RF signal mixed with the L.O., one is driven by a sinusoidal and one is driven by a cosinusoidal. The one driven by the sinusoidal is called the inphase(I) signal, and the one which is driven by the cosinusoidal is called the quadrature(Q) signal. The mixer output can be described by

$$I_{out,\cos} = I_p \cos \Box_m t \quad I_{out,\sin} = I_p \sin \Box_m t \tag{57}$$

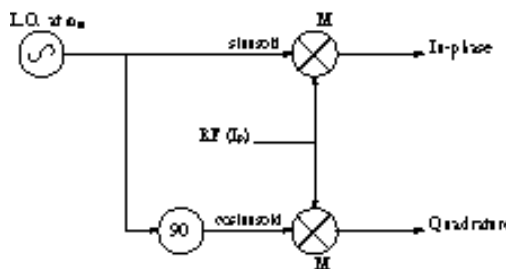


Figure 13. A schematic diagram of the RF signal measurement. Split up in a sinusoid and cosinusoid driven signal.

Mathematical analysis of the signal, driven by a cosinusoidal Eq. (57), follows

$$2 \operatorname{Re} [E_0 E_{\square 1}^* + E_1 E_0^*] e^{i \square_m t}$$

Assume $[E_0 E_{\square 1}^* + E_1 E_0^*] = a + ib$

$$\begin{aligned} & \square 2 \square \frac{1}{2} [(a + ib) e^{i \square_m t} + (a - ib) e^{-i \square_m t}] \\ & \square \frac{2d[e^{i \square_m t} + e^{-i \square_m t}]}{2} + \frac{2ib[e^{i \square_m t} - e^{-i \square_m t}]}{2} \\ & \square 2a \cos \square_m t \square 2b \sin \square_m t = I_p \end{aligned} \quad (58)$$

Multiplying I_p (in a mixer) with $\cos \square_m t$ will select ‘a’ (Real, inphase) and if multiplied with $\sin \square_m t$ will select ‘b’ (Imaginary, quadrature) of the output of the mixer.

$$\begin{aligned} V_I &= 2 \operatorname{Re} [E_0 E_{\square 1}^* + E_1 E_0^*] \quad \square \quad (\text{cosinusoidal}) \\ V_Q &= \square 2 \operatorname{Im} [E_0 E_{\square 1}^* + E_1 E_0^*] \quad \square \quad (\text{sinusoidal}) \end{aligned} \quad (59)$$

In Eq. (59) the two output signal are mathematically described. These signals are used to lock the cavity with the Pound-Drever frequency locking technique [11], which will be described in the next chapter.

The phase modulation in the signal is used to control the cavity. The phase modulation will give a amplitude change when the cavity is out of resonance. The shape of the error signal is given in Fig. 14, in the middle of the signal the cavity is at resonance. If the cavity deviates from resonance the phase modulation produces an amplitude change which will, electronically controlled, return the cavity to resonance.

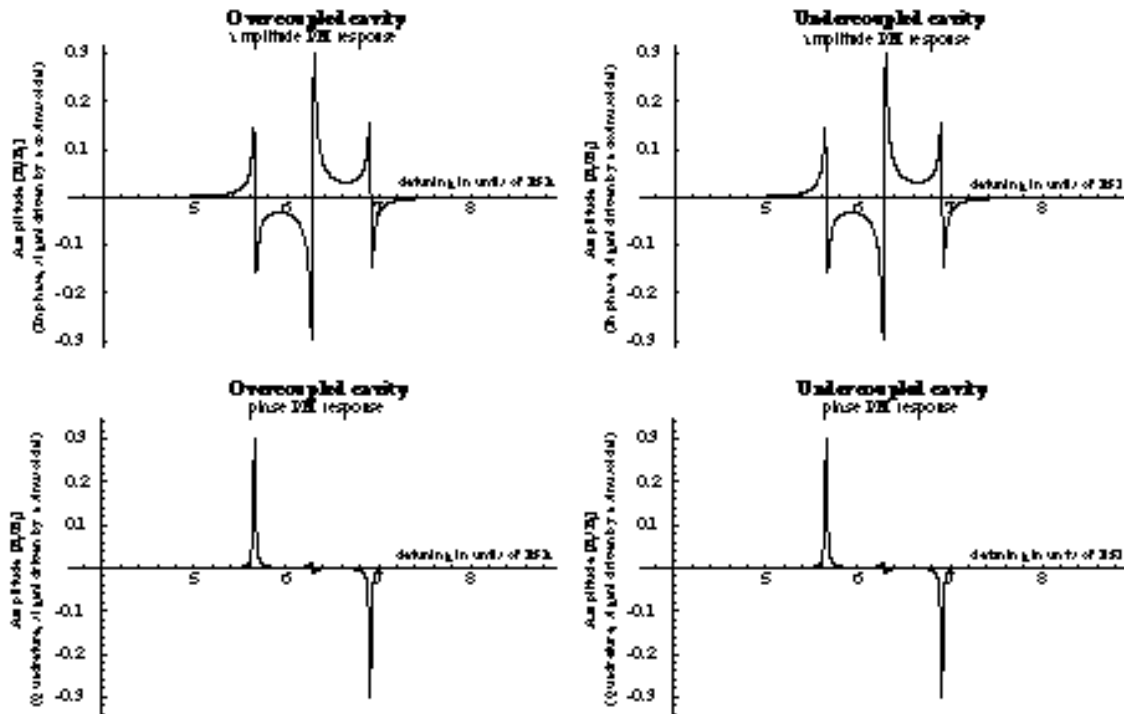


Figure 14. The shape of the phase modulation of an overcoupled cavity is the same as for an undercoupled cavity. That's why the amplitude modulation is used to detect the kind of cavity.

Chapter 6.

EQUIPMENT AND EXPERIMENTAL SETUP

The entire experiment was completed within 3 months, but the research and set up of the components took a longer time. This chapter describes the two main components of the set up, the laser and the cavity, as well as the other equipment used in the experiment. Then the complete set up is described along with the technique used to control the cavity.

6.1 The laser

The laser in the experiment was a diode pumped solid state ring laser (Lightwave 120), with an output power of 40 mW. A continuous wave (CW) laser diode pumps a Nd:YAG MISER (Monolithic Isolated Single-mode End-pumped Ring) crystal. The stability of the laser is obtained through its monolithic design and the mirrors of the laser cavity are the polished surfaces of the crystal. High mirror reflectivity is achieved through the use of either total internal reflection or through the application of optically reflective coatings to the surface of the crystal. A monolithic design, a stable laser diode pump, and coupled with the applied magnetic field of the crystal, provides the laser with an unidirectional operation. The non-planar beam path within the crystal is illustrated in Fig. 15.

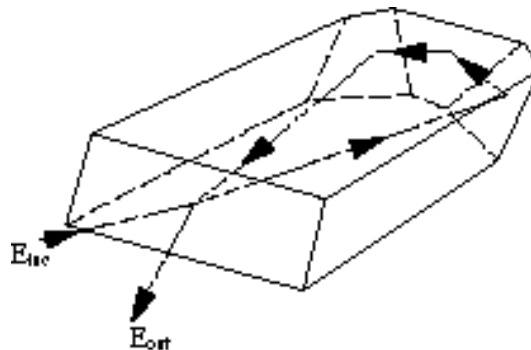


Figure 15. Out of plane beam path within the laser crystal

6.2 Other equipment^[10]

Three photodiodes used as illustrated in Fig. 16, one (PD3) is used to detect the transmitted field after the cavity. This photodiode is connected (DC output) to an oscilloscope to display the transmission peaks when the cavity is scanned, or is connected (RF output) to the spectrum analyser to display the FSR.

The other two photodiodes are used to detect the error signal from the cavity. Photodiode PD2 is used to detect all the data traces from the CRO (DC output) and the network

analyser (RF output). The CRO shows only the error signal and the network analyser shows the amplitude and the phase response of it. The photodiode PD1 is only used for the locking control loop. This transimpedance detector was used because it was limited to 10MHz which makes the locking signal cleaner

A network analyser and a spectrum analyser were used to collect most of the data. The network analyser was a Hewlett Packard HP-3589A. It produced an output signal which was used to drive the amplitude modulator or the laser diode. The modulated light was then detected by the photodiodes and was converted to a current which was detected by the network analyser. The network analyser displayed the relative phase and amplitude of the detected signal with respect to the output signal. This was used to detect and measure the reflected error signal, which was used to determine the kind of cavity. The network analyser is limited to produce and detect signals up to 150 MHz. The displayed traces (amplitude and/or phase) could be averaged over a number of detection cycles, removing transient effect (noise) from the result, and smoothing the plot. The resolution bandwidth (RBW) could be adjusted to vary the resolution of the displayed spectrum and the speed at which it was updated. The RBW specified the frequency span which was covered for each point that was plotted. A large RBW meant a low resolution (in frequency) plot but a fast update of the plot.

The spectrum analyser was a Hewlett Packard HP-8568B. The spectrum analyser detected the power spectrum of the time domain electrical signal. It was used to detect the transmitted signal which showed the FSR of the cavity. The input signal at the amplitude modulator was applied by an external signal generator, a Hewlett Packard HP-8444A-OPT 059 Both the spectrum analyser and the signal generator could detect and produce a signal up to 1.5 GHz. The displayed trace of the spectrum analyser could be averaged or have its RWB varied as for the network analyser.

Besides the spectrum and network analyser, a Hewlett Packard oscilloscope (CRO) was used to monitor the DC levels of the photo diodes (PD2 and PD3). A function generator produced a triangular signal which was amplified by a high voltage amplifier (± 100 V). The output from the high voltage amplifier was used to drive a PZT attached to one of the cavity mirrors to scan the cavity. A function generator operating at 9.1 MHz was used to phase modulate the laser and produce the locking signal, and a Proportional Integrating and Differentiating amplifier (PID), which produced the signal to control the locking of the cavity, was used also. All of the other electronic equipment used to modify the signal were Minicircuits products, power amplifiers (with a bandwidth of 500 MHz), amplifiers, attenuators, splitters/combiners, and mixers. The optical components were all anti-reflection (AR) coated for a wavelength of 1064 nm. They were mostly manufactured by Newport or CVI.

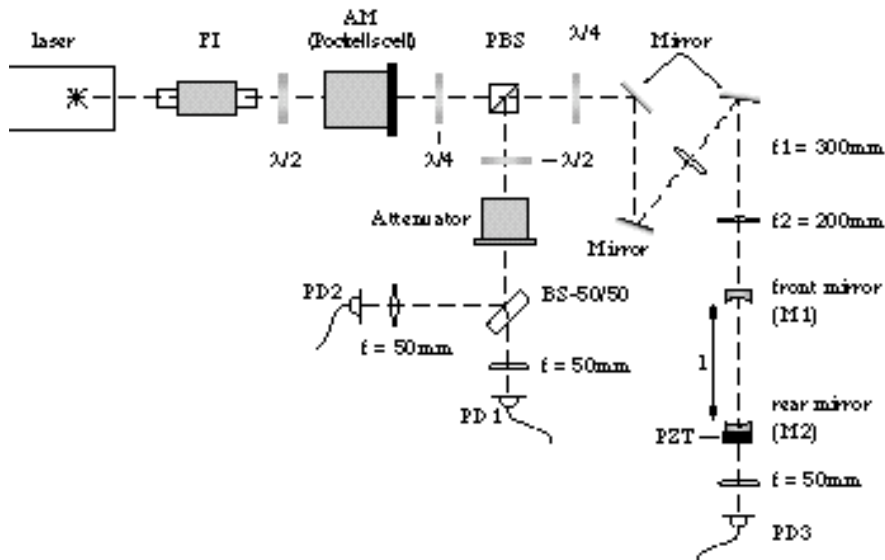


Figure 16. The optical bench top of the experiment.

6.3 The optical cavities

Three different cavities were compared in the experiment. As explained in chapter 3 a cavity can trap a Gaussian beam. Each cavity has its own Gaussian beam properties between the mirrors. The main property is the beam waist in the cavity, this is in the centre between the cavity mirrors. The incident beam on the cavity must have the same beam waist at the position where the cavity has its beam waist. Otherwise there is a ‘mode match’ between the incident laser beam and the cavity. For each mirror there could be two overcoupled and one undercoupled cavity build, each with different properties.

6.3.1 Cavity design

Each cavity, consisting of two curved mirrors, has its own properties. The different cavities were built using three different kinds of mirrors all with a Radius Of Curvature (ROC) equal to 1.5 meter. The main difference between the mirrors was the reflectivity varied, with a $R = 95\%$, $R = 98\%$ and a $R = R_{\max} (= \pm 99.7\%)$ mirror. Changing the reflectivity of the mirrors causes the finesse of the cavity to change. With these mirrors the finesse of the cavities is in the range of 100 to 300. The higher the finesse the more power is stored in the cavity.

The space between the mirrors, l , defines the free-spectral-range (FSR) of the cavity. The smaller l the higher the frequency between the fundamental modes of the cavity. The ROC of the mirrors is the base for the space between the higher order modes ($\square\square$) of the cavity. A cavity has its own waist size and position. The position of the waist in the cavity is always in the middle (for mirrors with equal ROC), between the mirrors, the size on the waist is dependent on the ROC and l . Below are the equations for the properties of the cavity.

$$FSR = \frac{c}{2L} \quad (15)$$

$$FWHM = \frac{FSR}{F} \quad (16)$$

$$F = \frac{\square(R_1 R_2)^{\frac{1}{4}}}{1 \square \sqrt{R_1 R_2}} \text{ (finesse)} \quad (17)$$

$$w_0^2 = \frac{\square}{2\square} \sqrt{l(2 \cdot ROC \square l)} \quad (60)$$

$$\square \square = FSR \cdot \frac{1}{\square} \cdot \cos^{\square} \square \square \frac{l}{ROC \square} \quad (61)$$

Table 1. The properties are calculated assuming, $l = 0.563 \text{ m}$, $\square = 1064 \text{ nm}$, $ROC = 1.5 \text{ m}$, $R1 = M1$ and $R2 = M2$.

	FSR [MHz]	FWHM [MHz]	F [-]	$\square \square$ [MHz]	$w_0 * 10^{-4}$ [m]
Cavity 1 $M1 = 95\%$, $M2 = R_{max}$	266.4	2.30	115.7	75.87	4.454
Cavity 2 $M1 = 98\%$, $M2 = R_{max}$	266.4	0.98	270.7	75.87	4.454
Cavity 3 $M1 = 98\%$, $M2 = 95\%$	266.4	3.03	87.9	75.87	4.454

Summed in Table 1, the FSR, $\square \square$ and the waist in the cavity are seen to be independent of the reflectivity of the mirror. If the reflectivity of the mirrors are unknown but the FWHM and the F are measured, then the reflectivity of the separated mirrors can be calculated.

To obtain the waist property of the beam in the cavity, the laser beam has to be focused in the middle of the cavity. If the properties of the output beam of the laser are known, and the waist size in the cavity is calculated, an optical set up can be designed. The Gaussian beam properties are used to determine the beam properties through the optical set up, the ABCD-law is used to calculate the position and focal lenght of the two lenses required. The amplitude modulator (AM), a Faraday Isolator (FI), a Polarisation Beam Splitter (PBS) and some wave plates ($\square/2$ or $\square/4$) are placed between the laser output and the first lens. The choice was made to use a 200mm and a 300mm lens, so that only the space between the lenses and the distance to the front mirror of the cavity had to be adjusted to produce the correct waist. The optical set up is illustrated in Fig. 16.

6.3.2 Cavity alignment

After the optical bench top was completed, the laser light had to be coupled into the cavity. When the light was coupled into the cavity and it was found that the mirrors were not well enough aligned a transmitted CRO-trace like Fig. 17(left) was displayed.

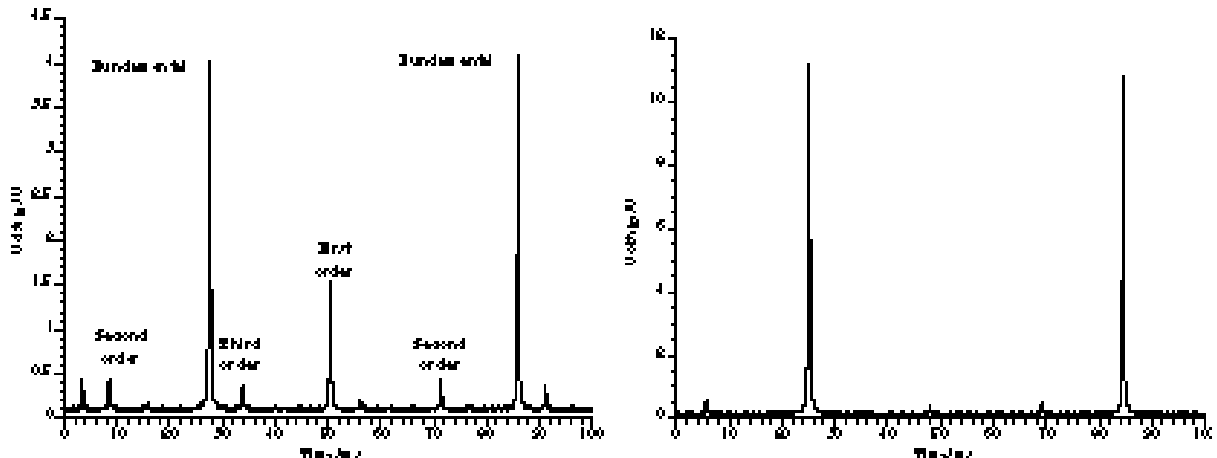


Figure 17. Oscilloscope trace of the transmitted power from the cavity while the cavity was scanned. Left when the cavity was misaligned and right when it was well mode-matched and aligned.

The transmission photo diode (PD 3 in Fig. 16) was connected to the CRO and a piezo element (PZT) on the rear mirror was connected to a function generator. The alignment of the photodiodes were done by position the focus of the 50 mm lenses in front of the detector. The function generator drove the piezo element, with a ± 100 Volt amplifier, to scan the cavity by changing the length of the cavity with the PZT. The length change of the PZT is linear to the voltage across the PZT.

By scanning the cavity the transmitted field can be described by Eq. (13). If the cavity is very well aligned, ie. there are no mode mismatch losses at all, a graphical plot of the transmitted field is very smooth, as in Fig 17 right. There are always losses in a cavity, on the input mirror and at the output mirror, absorption in the mirrors etc. If the cavity is misaligned higher order modes will appear. These higher order modes appear in the transmitted field as well as in the reflected field. After aligning the cavity, ideally the higher order modes are made to disappear. It is a matter to couple as much as possible light into the central mode by aligning the cavity. If the cavity is misaligned more light will be coupled into the higher modes. The most significant misalignments appear in the first and second order mode of the transmitted field. The first order mode represents a misalignment in the waist position of the x- and y-plane in the cavity. This can be controlled by tilting the mirrors until the first order mode on the CRO-trace is as small as possible (this correspond to the lowest DC level on the photodiode).

If the waist is not in the middle of the cavity, or the size does not match with the calculated cavity waist size, there will be light coupled into the second order mode. This can be controlled by shifting the mirrors or lenses in the z-axis (this is the direction of laser light propagation). The method used is as follows: The position of the mirrors is approximately known. Somewhere in the beam a aperture is placed, this aperture is big enough that the incident beam will just pass through it without clipping. The rear mirror is placed in this position such that the reflected beam from the mirror will pass through the aperture without

clipping. To correct the affect of the first mirror, as a negative lens, an AR coated input coupler is placed at the position of the front mirror. At the point of the aperture the incident beam and the reflected beam are equal in size. The same method is used to position the front mirror exclude of using the AR input coupler. The improvements are displayed onto the CRO-trace, by decreasing of the second order mode.

6.4 Frequency locking

The technique used in the experiment to control the cavity is known as Pound-Drever locking [11]. The laser light frequency is controlled at the same frequency as the cavity resonance frequency. In this technique the frequency of the laser is compared to the resonance frequency of the cavity and an error signal proportional to the difference is generated. A schematic diagram of the technique is illustrated in Fig. 18.

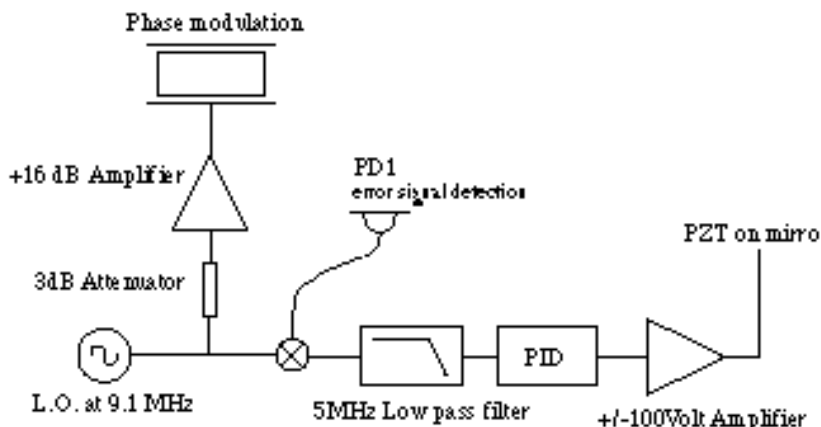


Figure 18. Schematic diagram of the Pound-Drever locking technique used in the experiment

The laser is aligned and modematched to the cavity and phase modulated at a frequency, Ω_m , which is large compare to the cavity optical bandwidth. The phase sidebands of the modulated light are therefore reflected from the cavity with no relative phase shift and detected on PD 1. In the experiment the cavity length is controlled by a piezoelectric transducer (PZT). Close to resonance, the reflection of the optical carrier experiences a strong phase shift [12]. When the phase modulated light reflected from the cavity is mixed with its sidebands, an amplitude modulated term at the modulation frequency is created, with an amplitude proportional to the sine of the round trip phase shift ($\Delta\phi$). Near resonance, the phase difference is very small, this term is then linearly related to the frequency offset [13][14],

$$\sin \Delta\phi \sim \frac{2\Delta\phi \Delta\phi_c}{FSR} \quad (62)$$

where $\Delta_f - \omega_c$ is the difference between the modulation frequency and the cavity resonance frequency.

The error signal is obtained by mixing the modulation frequency, produced by the LO, with the output of the detector PD1. The detected signal produced by the inphase mixer output is described and analysed in chapter 5, the shape of a typical error signal is shown in Fig. 19.

The slope of the error signal [V/Hz] on resonance represent the transfer coefficient from frequency to output voltage. If there is no frequency difference between the two frequencies, in the middle of the slope, then there is no voltage. The slope of the error signal is given by

$$D_v = \frac{8J_0(\Delta) J_1(\Delta)}{\Delta \omega_c} R_v P_i \quad (63)$$

where R_v is the detector responsivity in V/W, P_i is the effective input power in Watt, Δ is the modulation index and $\Delta \omega_c = c/2IF$, l is the length and F is the finesse of the cavity.

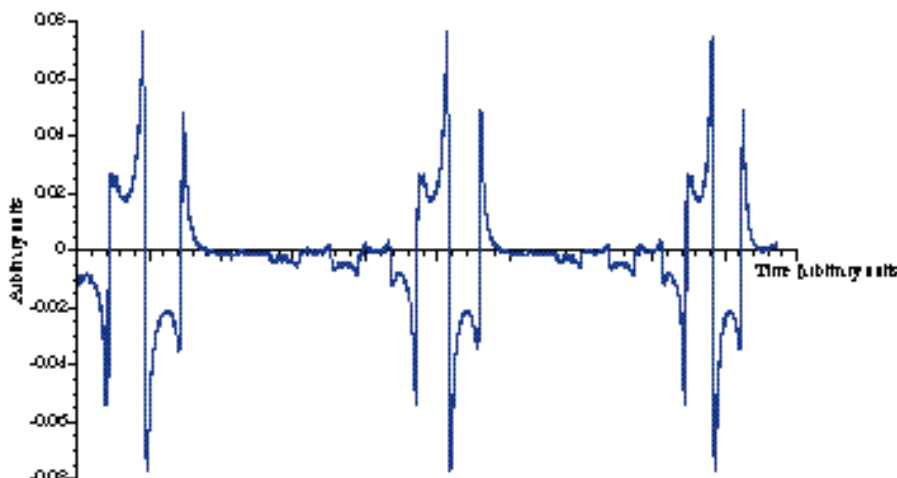


Figure 19. This is what the error-signal looks like.

When the system was setup, the locking control loop performed well. To lock the cavity the DC offset for the PZT was set, by tuning along the ± 100 Volt range of the amplifier. When the cavity length was at resonance the transmitted signal from PD3 dropped several volts on the CRO. Then the integrator was turned on to follow the error signal from PD1. The fine DC offset was used to fine tune the DC offset, this could be checked by the transmitted signal. The whole control loop was stable as long as the air between the mirrors was quiet and the optical table was not bumped. The locking servo remained effective until the dynamic range limit of the PZT was reached. When this occurred, it was necessary to manually relock the system to the next cavity mode.

Chapter 6. Equipment and experimental setup

Chapter 7.

EXPERIMENTAL RESULTS

All the data were capture via a GPIB interface in the computer, which was an Apple Macintosh with an interface card. The software were home build Lab View programs. The saved files were displayed by Delta Graph wherein the graphs were modified and redrawn with axes labels etc. The theoretical graphs were obtained by modelling the equation in Mathematica.

7.1 Cavity properties determination

The FSR and the FWHM of the cavity were obtained from the data of the spectrum analyser. The FWHM is at the point 3 dBm below the FSR. When these two parameters were gathered the finesse could be calculated with Eq. (16)

$$FWHM = \frac{FSR}{F} \quad \square \quad F = \frac{FSR}{FWHM} \quad (16)$$

This was done for all the cavities.

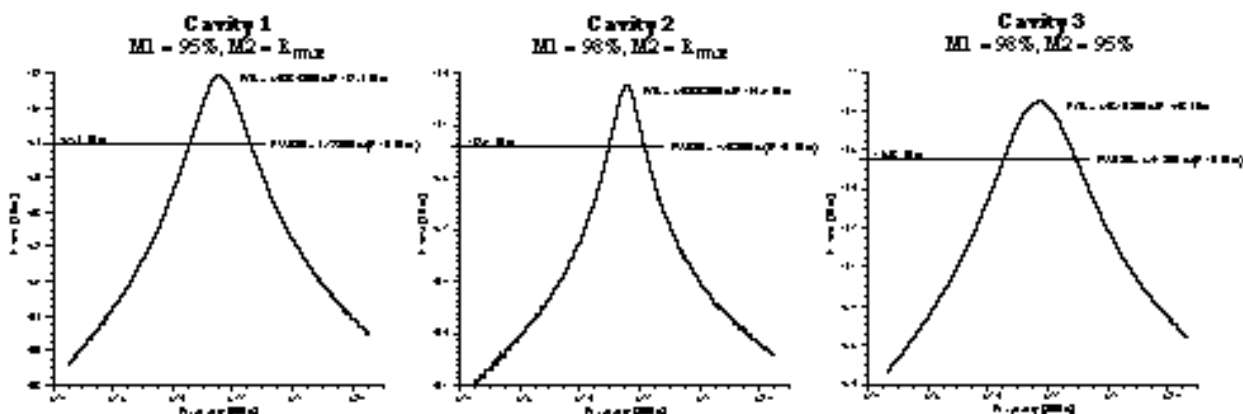


Figure 20. Traces from the spectrum analyser of the free spectral range (FSR) of the three different cavities. The FWHM of the FSR is 3 dB below the top , which was determined in the data of the graph.

Table 2. The measured finesses of the cavities.

	Cavity 1	Cavity 2	Cavity 3
Finesse [-]	159±0.02	408.5±3.3	109.2±0.2

An other method to determine the mirror reflectivity requires the gradient of the phase response of the error-signal. The gradient of the cavities where determine by looking to the

phase response of the network analyser of the three cavities, Fig. 21. From the data the gradients was determine by

$$s_x = \frac{\Delta\phi}{\Delta f} \cdot \frac{FSR}{360} \quad (64)$$

wherein $\Delta\phi$ is the phase difference of the phase response in degrees, Δf the frequency difference.

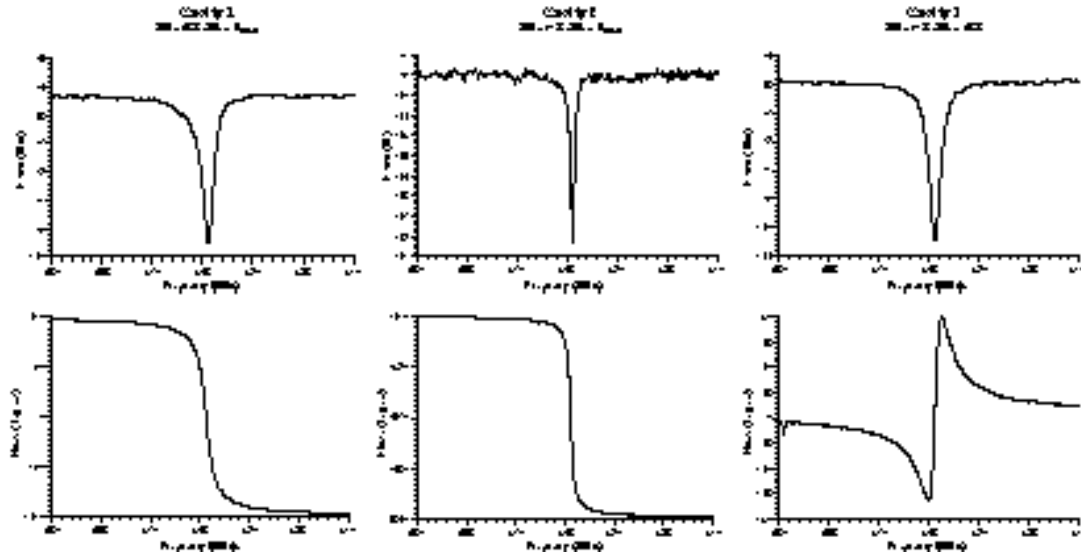


Figure 21. Traces from the network analyser with the phase response of the error-signals of the different cavities.

Table 3. The calculated slopes from the phase response.

	Cavity 1	Cavity 2	Cavity 3
gradient, s_x [deg/deg]	-133±2	-306±26	+38±1

7.2 Mirror reflectivity

The aim of this experiment was to determine the mirror reflectivity using the reflected beam and compare this data with that obtained from the transmitted beam. The calculations from the finesse was done by myself. The mirror calculations from the slope of the phase response of the error-signal was done by Karl who wrote a paper about this subject.

7.2.1 Calculations from the finesse

As shown before, the finesse could be calculated by the reflectivity of the mirrors in the cavity, described by (Eq. (17))

$$F = \frac{\sqrt{(R_1 R_2)^4}}{1 - \sqrt{R_1 R_2}} \text{ (finesse)} \quad (17)$$

wherein R_x are the amplitude reflectivity of the mirrors. When Eq. (17) is used for the three cavities there are three different equations with three unknown parameters as described below

$$\begin{aligned} 1 \quad & F_1^2 - 2F_1^2r_1r_3 + (F_1r_1r_3)^2 = 0 \\ 2 \quad & F_2^2 - 2F_2^2r_1r_2 + (F_2r_1r_2)^2 = 0 \\ 3 \quad & F_3^2 - 2F_3^2r_2r_3 + (F_3r_2r_3)^2 = 0 \end{aligned} \quad (65)$$

These equations were solved in Mathematica which give the following output for the three reflectivities:

$$r_1 = \frac{0.980448}{r_3} \quad r_2 = \frac{0.971693}{r_1} \quad r_3 = \frac{0.992339}{r_2}$$

which were then solved by hand, to give the values in table 4.

Table 4. The mirror reflectivities from the finesse.

	Manufactory reflectivity	Calculated reflectivity
R₁	95%	96.0±0.1%
R₂	98%	98.3±0.2%
R₃	R _{max} (99.7%)	100.1±0.2%

7.2.2 Calculations from the phase response

The idea of this experiment was to determine the reflectivity of the cavity mirrors by using the reflected field instead of the transmitted field. If the gradient of the phase response of the reflected field could be determined, the mirror reflectivity could be evaluated.

The reflected electric field is described by (Eq. (11))

$$\bar{E}_{R,\square} = \frac{A^2 - 2AB\cos\square + B^2}{1 - 2C\cos\square + C^2} \exp i \left[\tan^{-1} \frac{B\sin\square}{A - B\cos\square} \right] \tan \left[\frac{C\sin\square}{1 - C\cos\square} \right] \quad (11)$$

here $\bar{E}_{R,\square}$ is written in complex exponential notation. The phase response of the reflected field is given by the argument of $\bar{E}_{R,\square}$.

The gradient of the phase response of the reflected field is described by

$$\frac{\partial \arg(\bar{E}_{R,\square})}{\partial\square} = \frac{AB\cos\square - B^2}{A^2 - 2AB\cos\square + B^2} \left[\frac{C\cos\square - C^2}{1 - 2C\cos\square + C^2} \right] \quad (66)$$

wherein A, B and C are described in Chapter 3.1 and are substitute from the reflectivity of the mirrors. When the cavity is on resonance the round trip phase of the circulating light in the cavity is zero, $\Delta=0$, the gradient of the phase response can be simplified to,

$$s_x = \frac{\partial \arg(\bar{E}_{R,\Delta})}{\partial \Delta} = \frac{r_2 t_1^2}{(1 - r_1 r_2)(r_1 - r_2(r_1^2 + t_1^2))} \quad (67)$$

where in s_x is the gradient of the different cavities, r_2 the amplitude reflectivity of the rear mirror, r_1 the amplitude reflectivity of the front mirror and t_1 the amplitude transmission of the front mirror, which must be measured with a power meter.

Table 5. The mirror reflectivity from the slope of the phase response of the error-signal.

	Measured transmission (T_x)	Manufactory reflectivity	Calculated reflectivity
R ₁	3.1±0.02%	95%	96.2±0.2%
R ₂	1.3±0.1%	98%	98.6±0.2%
R ₃	0.15±0.02%	R _{max} (99.7%)	99.9±0.2%

7.3 The calculations

All the calculations were done in Mathematica or MATLAB with programs written by Karl and myself. The programs where first tested before the data was used for further calculations.

Chapter 8.

CONCLUSION

If the information of the transmitted and reflected signal are compared there are several advantages and disadvantages. The reflected signal is more useful when a super high finesse cavity is used, or when the cavity is used as a mode cleaner, no beam splitters after the cavity. On the other hand the finesse is more reliable from the transmitted signal. The signal to noise ratio from the reflected signal is not as high as that from the transmitted signal.

The property which only can be determined from the reflected signal is the type of coupling onto the cavity. This is impossible from the transmitted signal (see Figures 4 and 5 in chapter 3). An overcoupled cavity gives a qualitatively different signal response compared to an undercoupled cavity.

The method to analyse the data from the reflected signal is much more complicated than of the transmitted signal, which can be a disadvantage. With both techniques the identification of the higher order modes is possible.

Chapter 8. Conclusion

A closer examination of the Fabry-Perot Interferometer

BIBLIOGRAPHY

- [1] A. Yariv, "Optical Electronics", chapter 2, 3rd edition, CBS College Publishing, New York, 1985.
- [2] A. E. Siegman, "Lasers", chapter 15, University Science Books, Mill Valley, 1986.
- [3] A. E. Siegman, "Lasers", chapter 17, University Science Books, Mill Valley, 1986.
- [4] Hewlett-Packard, "Fibre Optics Handbook", 2nd edition.
- [5] Peter K. Fritschel, "Techniques For Laser Interferometers Gravitational Wave Detection", PhD thesis, Massachusetts Institute of Technology, 1992.
- [6] A. Yariv, "Optical Electronics", chapter 4, 3rd edition, CBS College Publishing, New York, 1985.
- [7] Ferrel G. Stremler, "Introduction to Communication Systems", chapter 5, 2nd edition, Addison-Wesley Publishing Company, 1977.
- [8] Ferrel G. Stremler, "Introduction to Communication Systems", chapter 6, 2nd edition, Addison-Wesley Publishing Company, 1977.
- [9] A. Yariv, "Optical Electronics", chapter 9, 3rd edition, CBS College Publishing, New York, 1985.
- [10] Karl G. Baigent, "Automatic Modematching of a Laser Beam into an Optical Cavity", Bachelor thesis, Australian National University Dept. of Physics and Theoretical Physics, 1996.
- [11] R. W. P. Drever, J. L. Hall, F. V. Kowalski, J. Hough, G. M. Ford, A. J. Munleyand and H. Ward, "Laser Phase and Frequency Stabilisation using an Optical Resonator", Applied Physics B 31, 97-105, 1983.

A closer examination of the Fabry-Perot Interferometer

- [13] T. Day, E. K. Gustafson and R. L. Byer, “Sub-Hertz relative frequency stabilisation of two diode laser pump Nd:YAG lasers locked to a Fabry-Perot interferometer”, IEEE Journal of Quantum Electronics, Vol. 28, no. 4, page 1106-1117, 1992.
- [12] A. E. Siegman, “Lasers”, chapter 11, University Science Books, Mill Valley, 1986.
- [14] Malcolm B. Gray, “Quantum Noise Limited Interferometer”, PhD thesis, Australian National University Dept. of Physics and Theoretical Physics, 1995.